Marine Structures 84 (2022) 103205

Contents lists available at ScienceDirect

Marine Structures

journal homepage: www.elsevier.com/locate/marstruc

The effect of the yield to tensile strength ratio on stress/strain concentrations around holes in high-strength steels

Siemen F.P.M. Obers [a,b], Jaap J. Overal [b], Wei Jun Wong [a,*], Carey L. Walters [a]

[a] Department of Maritime and Transport Technology, Delft University of Technology, Mekelweg 2, 2628 CD Delft, The Netherlands
[b] Huisman Equipment B.V., Admiraal Trompstraat 2, 3115 HH Schiedam, The Netherlands

ARTICLE INFO

Keywords:
SCF
Elasto-plastic
Ultra high-strength steels
Y/T

ABSTRACT

Application of high-strength steels in the maritime and offshore industry is currently limited by rules governing the ratio of the yield to tensile strength (the Y/T ratio). To better understand the physical basis for these rules, the nature and extent of the plastic stress/strain field in the vicinity of a stress concentration (a circular hole) in a structure made from high-strength steel are analyzed. This is done through analytical models of the stress field and the extent of plasticity in the vicinity of a hole based on classical methods. These analytical methods are validated through FEA models that are in turn validated by published experimental data. This paper concludes that a high Y/T ratio leads to a lower plastic SCF and a higher local strain in the vicinity of a hole. The extent of the plastic zone is not affected by different values of Y/T ratio for different values of σ_{nom}/σ_y.

1. Introduction

Over the years, new, high-strength (σ_y > 550 MPa) and ultra high-strength (σ_y > 780 MPa) steels have found their way into the maritime and offshore industry in applications such as jack-up structures, submarines, mooring chains, pipelines, pipe-lay towers, lifting appliances and icebreakers [1,2]. These steels are attractive because they are stronger and therefore require less material to achieve the same result: a safely designed structure. The introduction of high-strength steels also brings challenges with respect to rules because limits are set for the yield to tensile strength (Y/T) ratio to ensure structural safety [3–5]. For example, the Y/T ratio is restricted to a maximum of 0.94 for steel grades with yield strengths between 420 and 960 MPa in [3–5]. But in practice, such high-strength steels are sometimes delivered with higher Y/T ratios than deemed acceptable by the rules. This problem is further exacerbated by steels that have higher-than-specified yield stresses, resulting in higher overall strength but also a higher Y/T ratio. Several failure modes have been identified in which the yield to tensile strength ratio plays a role [6]. All of these failure modes require further development in order to understand the impact of high yield to tensile strength ratios on safety. The purpose of this paper is to focus on one of those specific modes, specifically the concentration of stresses and strains in the presence of a stress concentration. Understanding the influence of yield to tensile strength ratio can help to give the basis for more scientifically-grounded rules. Specifically, this paper focuses on the stress field in stress/strain concentrations around holes in steel structures to ultimately find the effect of the Y/T ratio on the tendency of steels with a high Y/T ratio to concentrate stresses and strains. This has tremendous practical value because nominal design stresses are often 2/3 of the yield stress [4,7,8], but it is well-known that the stress concentration factor in an elastic structure is 3 [9]. This leads to the conclusion that yielding is likely present in the vicinity of circular holes at nominal stresses far below the design stress.

* Corresponding author.
E-mail address: W.J.Wong@tudelft.nl (W.J. Wong).

https://doi.org/10.1016/j.marstruc.2022.103205
Received 20 October 2021; Received in revised form 25 January 2022; Accepted 4 March 2022

Nomenclature

ϵ	Strain
ϵ_{eng}	Engineering strain
ϵ_{local}	Local (true) strains acting in the angular (θ) direction at the hole
ϵ_{peak}	Peak (true) strain acting in the angular (θ) direction at the hole, at $\theta = \pi/2$ and r/a
ϵ_{true}	True strain
$\epsilon_{u,eng}$	Engineering ultimate stress
$\epsilon_{u,true}$	True ultimate stress
$\epsilon_{y,eng}$	Engineering yield strain
$\epsilon_{y,true}$	True yield strain
ϵ_y	Yield strain
σ	Stress
σ_θ	Stress acting in the angular (θ) direction at circular hole
σ_{eng}	Engineering stress
σ_{nom}	Nominal applied stress
σ_{true}	True stress
$\sigma_{u,eng}$	Engineering ultimate stress
$\sigma_{u,true}$	True ultimate stress
$\sigma_{y,eng}$	Engineering yield stress
$\sigma_{y,true}$	True yield stress
σ_y	Yield stress
θ	Angular coordinate at circular hole
a	Radius of circular hole
E	Young's modulus
e	Euler's number
E_s	Secant modulus
$E_{s,\infty}$	Secant modulus far away from the stress concentration
K	Strength coefficient of the Hollomon law
n	Strain hardening exponent of the Hollomon law
R	Shift of the elastic stress field to accommodate the plastic stress field
r	Radial coordinate at circular hole
r_p	Radius at which the analytical elasto-plastic stress distribution transitions from purely elastic behavior to yielding (the extent of the plastic zone)
r_y	Radius at which the classical elastic stress distribution at a hole exceeds the yield stress
SCF	Stress concentration factor
Y/T	Yield to tensile strength ratio, based on engineering stress

Stowell analytically described the plastic stress concentration around a circular cutout in an infinite plate under uniform tension for an incompressible material [10]. The stress concentration described by Stowell is not directly related to the Y/T ratio. The authors are unaware of any prior studies in which the influence of the Y/T ratio is analyzed for the tendency to develop strain localizations in the vicinity of circular holes at nominal stresses below and above the design stress.

This work will develop elasto-plastic analytical models that relate the Y/T ratio to the stress/strain field for a circular cutout under uniform tension based on of Stowell's work. Analytical models are preferred for their ease of use and potential for giving insights into general trends. The analytical models will be validated with numerical models.

The analytical treatment is described in Section 2, where the plastic stress/strain distribution occurring around a hole given by Stowell [10] is developed to find the dependence of the stress distribution on the Y/T ratio using the equation of Leis [11], together with an estimate for the extent of the plastic zone inspired by Irwin [12]. Then, the numerical model is discussed in Section 3, which includes its validation against experimental data and the validation of the analytical methods. Section 4 gives a parametric study based on this analytical model, to assess the influence of yield strength and Y/T ratio independently from each other. Finally, a conclusion is drawn in Section 5.

2. Elasto-plastic analysis of a circular cutout using an analytical model

In this section, the existing relationship for the stress field around a circular cutout [10], originating from the classical elastic solution, is updated to include the Y/T ratio. This is done by assuming the Hollomon hardening rule [13] and applying a known relationship between the hardening rule parameters and the Y/T ratio [11].

2.1. Development of the plastic SCF

Analytical relationships describing the stress concentration factor (SCF) are available [10,14,15]. However, an analytical relationship between the SCF and the Y/T does not exist. This section shows how this relationship could be found by first relating the Y/T ratio to the strain hardening exponent n as shown in Leis [11], then updating the analytical SCF expressions to be expressed in terms of n, and finally using the relationship between n and Y/T to relate the SCF to Y/T.

To obtain a relationship between Y/T and n, Leis [11] first assumes a material law as given by Hollomon (Eq. (1)) [13].

$$\sigma_{true} = K \cdot \epsilon_{true}^{n} \tag{1}$$

Here, σ_{true} is the true stress, ϵ_{true} is the true strain, and K and n are material constants. When Eq. (1) is substituted into the Considère condition [16]:

$$\sigma_{true} = \frac{\partial \sigma_{true}}{\partial \epsilon_{true}} \tag{2}$$

The true strain at the onset of necking is found:

$$\epsilon_{u,true} = n = \ln(1 + \epsilon_{u,eng}) \tag{3}$$

Where the subscript u indicates the strain corresponding to the ultimate stress. Therefore, the engineering strain corresponding to the ultimate stress is:

$$\epsilon_{u,eng} = e^{n} - 1 \tag{4}$$

Rewriting Hollomon's law using the Considère condition [16] results in an expression for the strength coefficient, K, given in Eq. (5).

$$K = \frac{\sigma_{u,true}}{n^{n}} \tag{5}$$

Substituting Eq. (5) into Eq. (1) and evaluating at the resultant equation at the yield point gives:

$$\frac{\sigma_{y,true}}{\sigma_{u,true}} = \left(\frac{\epsilon_{y,true}}{n}\right)^{n} \tag{6}$$

The relationships for converting true stress and strain into engineering stress and strain are:

$$\sigma_{true} = \sigma_{eng} \cdot (1 + \epsilon_{eng}) \tag{7}$$

$$\epsilon_{true} = \ln(1 + \epsilon_{eng}) \tag{8}$$

The Y/T ratio is typically stated in terms of engineering stress and strain, so the Y/T ratio is:

$$\frac{Y}{T} := \frac{\sigma_{y,eng}}{\sigma_{u,eng}} = \frac{1}{1 + \epsilon_{y,eng}} \cdot \left(\frac{e \cdot \ln(1 + \epsilon_{y,eng})}{n}\right)^{n} \tag{9}$$

Eq. (9) was developed by Leis [11] and is referred to hereafter as the Leis equation.

Hollomon's power law tends to under-predict the yield stress in roundhouse stress–strain curves and certainly in stress–strain curves with Lüder's plateaus. As the stress–strain curves for high-strength steels have roundhouse stress–strain curves, the under-prediction is limited.

The classical elastic solution of the SCF of a circular cutout in an infinite plate under far-field tension is given in Eq. (10) [14].

$$\frac{\sigma_{\theta}}{\sigma_{nom}} = \frac{1}{2}\left(1 + \frac{a^2}{r^2} - \left(1 + \frac{3a^4}{r^4}\right)\cos 2\theta\right) \tag{10}$$

Stowell updated Eq. (10) into an analytical approximation of the plastic solution of the SCF for a circular cutout under uniform tension shown in Eq. (11).

$$\frac{\sigma_{\theta}}{\sigma_{nom}} = \frac{1}{2}\left(1 + \frac{a^2}{r^2} - \frac{E_s}{E_{s,\infty}} \cdot \left(1 + \frac{3a^4}{r^4}\right)\cos 2\theta\right) \tag{11}$$

Where a is the radius of the hole, r is the distance from the center of the hole, θ is the angle relative to the tensile axis, E_s is the secant modulus, σ_{θ} is the stress in the θ-direction, and σ_{nom} is the nominal stress. The nominal stress is calculated with the gross cross-section of the specimen, without taking the discontinuity into account. Fig. 1 is a schematic representation of the hole and geometric parameters. The far-field secant modulus $E_{s,\infty}$ is equal to the Young's modulus E, since no global yielding is assumed.

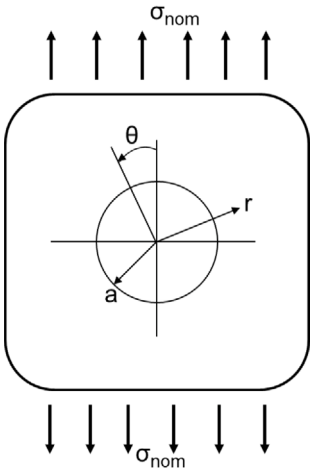

Fig. 1. Circular cutout subjected to uniform tension.

By definition, the secant modulus is the stress divided by the strain, so the secant modulus for Hollomon's law is:

$$E_s = K \cdot \epsilon^{n-1} \tag{12}$$

Solving Hollomon's law for ϵ and substituting into Eq. (12) gives:

$$E_s = K \cdot (\frac{\sigma}{K})^{\frac{n-1}{n}} \tag{13}$$

Assuming that the yield point occurs at the intersection of the linear elastic region and Hollomon's equation:

$$E \cdot \epsilon_y = K \cdot \epsilon_y^n \tag{14}$$

Eq. (14) results in an unique expression for the strength coefficient:

$$K = E \cdot (\frac{\sigma_y}{E})^{1-n} \tag{15}$$

When Eq. (15) is substituted into Eq. (13) and normalized by E, the ratio E_s/E is found:

$$\frac{E_s}{E} = (\frac{\sigma}{\sigma_y})^{\frac{n-1}{n}} \tag{16}$$

Substituting the definition of the Stress Concentration Factor (SCF) (i.e. the ratio of the local stress to the nominal stress) into Eq. (16) yields:

$$\frac{E_s}{E} = (SCF \cdot \frac{\sigma_{nom}}{\sigma_y})^{\frac{n-1}{n}} \tag{17}$$

Substituting this ratio into the Stowell equation in Eq. (11) results in Eq. (18).

$$SCF = \frac{1}{2}\left(1 + \frac{a^2}{r^2} - (SCF \cdot \frac{\sigma_{nom}}{\sigma_y})^{\frac{n-1}{n}} \cdot (1 + \frac{3a^4}{r^4}) \cdot \cos 2\theta\right) \tag{18}$$

Eq. (18) gives the distribution of the SCF with varying coordinates (r, θ), for given material properties σ_y and n, at different levels of applied loading σ_{nom}. Since the peak stresses and strains which are of interest occur at the cut along $\theta = \pi/2$, the analyses and discussion in the subsequent sections are applied to that cut. This is done by making the substitution $\theta = \pi/2$ and then solving the implicit equation for the SCF numerically. Applying Eq. (9) gives this elasto-plastic SCF as a function of the Y/T ratio. Finally, to describe the region where the material is expected to be linear elastic and where the extent of the plastic zone theoretically terminates, the shift in the classical elastic stress field as described in Section 2.3 is applied.

2.2. Local strain

Substituting Eq. (12) and $E_{s,\infty} = E$ into Eq. (11) gives the stress field in terms of strain:

$$\frac{\sigma_\theta}{\sigma_{nom}} = \frac{1}{2}\left(1 + \frac{a^2}{r^2} - \frac{K \cdot \epsilon_{local}^{n-1}}{E} \cdot (1 + \frac{3a^4}{r^4}) \cos 2\theta\right) \tag{19}$$

Solving for the local strain and evaluating at location $\theta = \pi/2$ and $r/a = 1$, as the highest strain occurs at this point, results in Eq. (20).

$$\epsilon_{peak} = ((\frac{1}{2} \cdot SCF - \frac{1}{2}) \cdot \frac{E}{K})^{\frac{1}{n-1}} \tag{20}$$

2.3. Estimation of the plastic zone size

As described in Section 2, in order to express the stress distribution in a form which uses the strain hardening exponent n and σ_y as the only material parameters (without E_s or K) (Eq. (18)), so that this could then be related to Y/T through Leis (Eq. (9)) [11], the Hollomon curve was used together with the assumption that the curve passes through the yield point on the linear elastic stress–strain line (Eq. (14)). This results in a material behavior which below yielding has, instead of a linear elastic behavior, a curved relation resulting in over-prediction of those pre-yield stresses. The resulting elasto-plastic stress distribution is hence one which is applicable for the plastic region but which over-predicts stresses for the elastic region. This section describes the method used to approximate the extent of the plastic zone over which the preceding Hollomon-based derivation applies, given by the radius r_p along $\theta = \pi/2$, at which the behavior switches between linear-elastic and plastic. Once this location is found, it is known that for radii r past this point, the behavior is simply that of the classical elastic solution (Eq. (10)), which is shifted to line up with r_p to give a continuous distribution.

Inspired by fracture mechanics, the extent of the plastic zone is estimated by finding how wide the plastic zone would have to be in order to have the same net force as the equivalent elastic strain field [12]. In this portion of the analysis, an elastic-perfectly plastic material is assumed. The elastic-perfectly plastic solution gives a conservative upper bound of the extent of the plastic zone, and the suitability of this assumption is discussed together with the results in Section 4. Fig. 2 shows the load that needs to be redistributed. Here, r_y is the radius over which the elastic solution is greater than the yield strength, r_p is the extent of the plastic zone necessary to maintain force balance, σ_θ is the stress in the θ-direction along the $\theta = \pi/2$ axis, and σ_y is the yield stress.

The expression for r_y can be found by setting the σ_θ into the elastic solution (Eq. (10)) equal to the yield stress and assuming $\theta = \pi/2$.

$$\frac{a}{r_y} = \sqrt{-\frac{1}{6} + \frac{1}{3}\sqrt{-\frac{23}{4} + 6 \cdot \frac{\sigma_y}{\sigma_{nom}}}} \tag{21}$$

From there, force balance can be used to find r_p. This can be found by:

$$\sigma_y \cdot r_p = \int_0^{r_y} \sigma_\theta dr \tag{22}$$

Solving Eq. (22) for r_p gives:

$$\frac{r_p}{a} = \frac{\sigma_{nom}}{\sigma_y} \cdot (\frac{r_y}{a} - \frac{1}{2} \cdot \frac{a}{r_y} - \frac{1}{2} \cdot (\frac{a}{r_y})^3) + 1 \tag{23}$$

Assuming that the extent of plasticity is given by Eq. (23) (which is larger than Eq. (21)) means that the plastic solution will no longer transition smoothly to the elastic solution at the edge of the plastic zone. Therefore, the elastic stress field will be shifted so that it is continuous with the edge of the plastic zone. This will be accomplished by replacing r in Eq. (10) with R:

$$R = r - (r_p - r_y) \tag{24}$$

The concept of R as a new origin for the elastic solution which has been shifted to accommodate the plastic stress field is demonstrated in Fig. 2.

3. Numerical validation of the plastic SCF solution

In this section, the analytical plastic SCF solution is validated by comparison with a finite element analysis (FEA). The FEA model is made with Ansys 2020 [17], and it is compared with tensile tests performed on an S960 steel in [18], for both the situations with and without a hole. Toward that end, the material model is first discussed, followed by the development and experimental validation of the numerical model. The model is then modified to be more comparable to the theoretical model, and the results are then compared with the theoretical model itself.

3.1. Material model

Local strains beyond the necking strain will be possible in this model, so the true stress–strain relationship beyond the onset of necking in a standard tensile test is needed. The traditional methods of correcting engineering stress and strain to true stress and strain cannot be applied beyond the onset of necking, so an inverse engineering approach will be used. In this approach, The material's true stress–strain curve as described by the Hollomon law (Eq. (1)) is used as an input to the finite element model of the tensile test, from which an engineering stress–strain curve (based on gage length) is obtained and used for comparison with the experimental engineering stress–strain curve obtained from [18]. The parameters K and n of the Hollomon law are iteratively changed until there is a 5% match between the experimental and finite element engineering stress–strain curves. This engineering stress–strain curve obtained from FEA based on the calibrated K and n parameters is shown in Fig. 3, alongside the experimental results from [18]. The material properties and fitting parameters are given in Table 1.

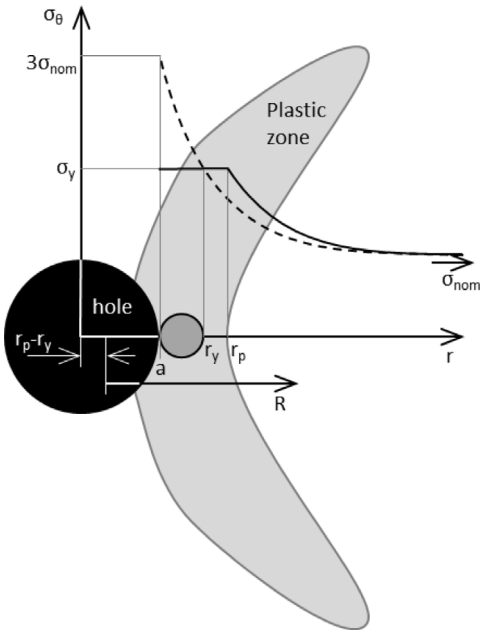

Fig. 2. Schematic of the plastic zone near the hole, compared to the elastic solution and perfectly plastic solution.

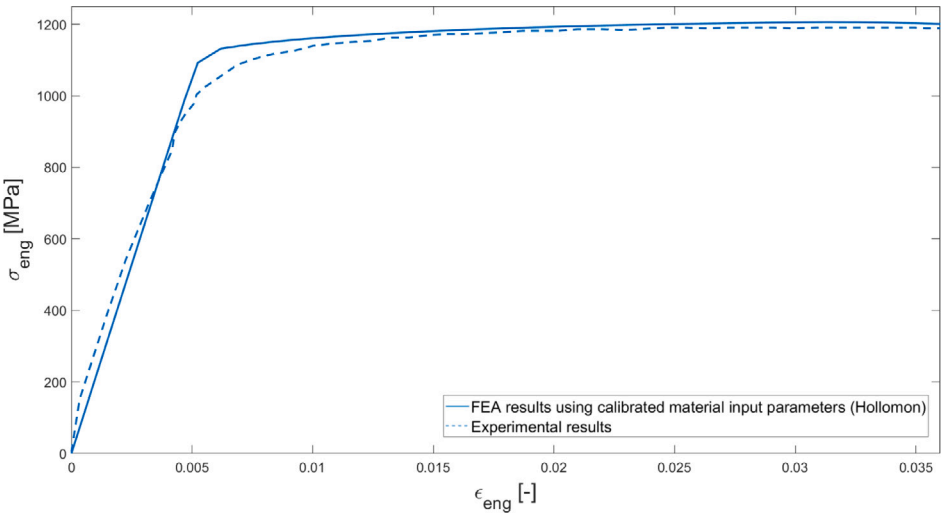

Fig. 3. Standard tensile test engineering stress–strain curve S960 — plain steel specimen; experimental results from [18].

Table 1
S960 material properties and fitting parameters.

	Value	Unit
Steel grade	S960	[–]
Young's modulus	210	[GPa]
$\sigma_{y,eng}$	1084	[MPa]
$\sigma_{u,eng}$	1191	[MPa]
Y/T	0.91	[–]
K	1490	[MPa]
n	0.055	[–]

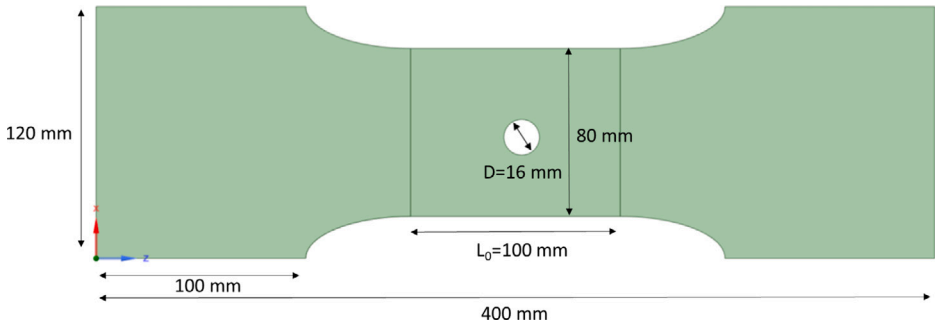

Fig. 4. Tensile test specimen with a thickness equal to 8 mm.
Source: from [18]

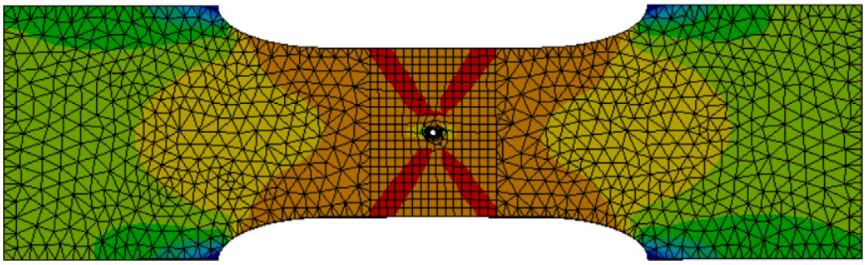

Fig. 5. Numerical model with a thickness equal to 8 mm.

3.2. Numerical modeling and validation

The calibrated material properties, found by reverse engineering of the tensile test (without hole) as described in Section 3.1, are applied to the simulation of a tensile test containing a 16 mm circular hole (Fig. 4), involving the same steel from the same test database [18]. The applicability of this calibrated material model to the situation with a hole is verified in Section 3.3 below by comparison with the corresponding experiment.

Having established its validity based on this experimental comparison, the finite element model could then be used to make comparisons against predictions given by the analytical model described in Section 2 above, when applied to the same situation of a circular hole of 16 mm diameter. Since the analytical model is based on a plate with an infinite width, when making comparisons with the analytical model, the width and length of the finite element specimen are scaled up, while maintaining the size of the circular hole and the specimen thickness. The appropriate amount of scaling is determined by the balance between computational times and achieved level of agreement between the theoretical and numerical results. Hence, the width of the ligaments and the total length are here scaled by a factor of six (Fig. 5), resulting in an FEA specimen with a total length of 2400 mm and total width at the gauge section of 400 mm. The scaling changed the width-to-hole-diameter ratio from 5 in the experiment to 25 in the subsequent simulations, which was a substantial improvement.

The specimen is simulated using Ansys 2020 software, with SOLID187/SOLID186 (quadratic hexahedron and tetrahedron) elements (Fig. 5). The element size near the hole was 0.5 mm, representing 16 elements over the thickness. A refined, unstructured mesh extended in the width direction to an r/a ratio of approximately 1.6, then transitioned to a more coarse mesh. A remote displacement is imposed on the end of the specimen in the longitudinal direction. One side of the specimen is fully clamped, and the other is fully clamped except for the degree of freedom in which the displacement was imposed. A minimum mesh size of 2 mm was used, and it was shown to calculate a peak stress within 1% of a finer mesh.

3.3. Experimental validation

Simulating the geometry shown in Fig. 4 and calculating an engineering strain with a gauge length of 100 mm, centered on the hole, results in the engineering stress–strain curve shown in Fig. 6. This figure shows the similar behavior for the experimental data obtained from [18], and an overestimation of the stress–strain behavior approximately equal to 5% is observed. The 0.2% offset yield stresses obtained from the experimental and finite element results for this holed geometry are 1129 MPa and 1190 MPa, respectively, and the ultimate stresses are 1169 MPa and 1217 MPa, respectively.

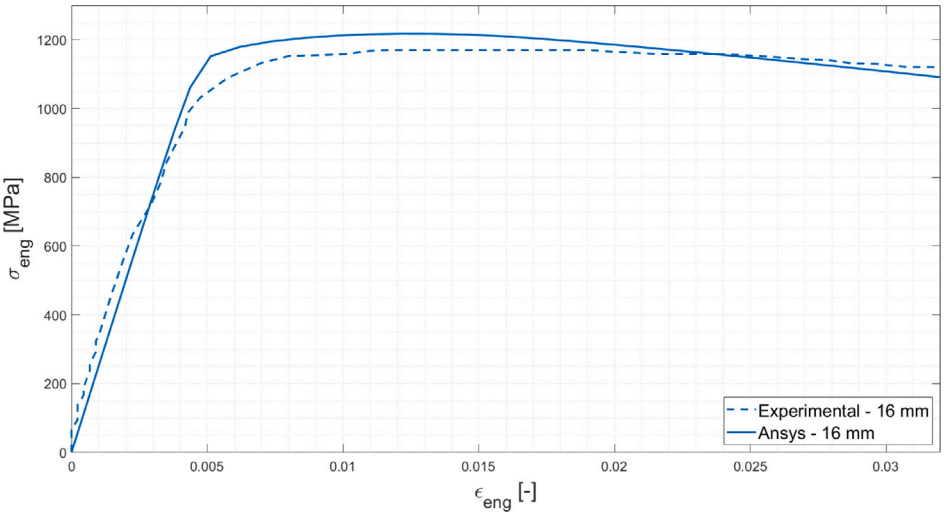

Fig. 6. Standard tensile test engineering stress–strain curve S960 — specimen with circular cutout of 16 mm; experimental data from [18].

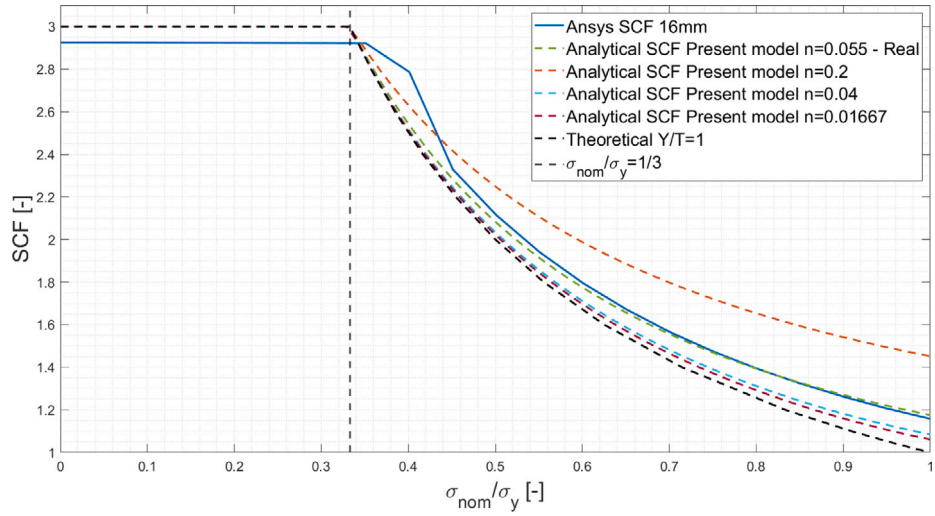

Fig. 7. SCF as function of normalized nominal stress for S960 with Y/T = 0.91 — analytical versus numerical.

3.4. Comparison between analytical and numerical model

In this section, the equations from Section 2 are compared to the calibrated numerical models. The ligaments from the specimen shown in Fig. 5 were scaled from 32 mm up to 192 mm in order to more closely approximate the infinite plate theory that Eqs. (11) and (19) were based on. Eq. (18) is compared with the finite element results for S960 steel in Fig. 7. This figure shows a constant SCF of 3 until σ_{nom}/σ_y equals 1/3 for the theoretical elastic solution [9]. The elastic SCF for the numerical solution is less than the theoretical value of 3 due to the finite width. Up to a value of σ_{nom}/σ_y of 1/3, the material behaves elastically. After this point, the plastic SCF decreases due to redistribution of strain. This decrease in plastic SCF is well captured by the analytical Stowell approximation. An elastic-perfectly plastic solution in which no hardening occurs is also presented in Fig. 7. The perfectly plastic solution (Y/T = 1) is derived from the observation that the maximum stress is the yield stress, so the SCF is given by $SCF = \sigma_y/\sigma_{nom}$.

A comparison is made between Eq. (20) and the FEA results of the local strain at location $\theta = \pi/2$ and $r/a = 1$, in Fig. 8. The strain hardening exponent in Eqs. (18) and (20) is varied to show the influence. The analytical formulation is able to approximate the strain behavior relatively accurately. The inconsistency in the numerical solution when σ_{nom}/σ_y is 0.36 is not shown in the analytical solution, which causes a systematic overestimation. The strain hardening exponent equal to 0.055 corresponds to the real material, the other exponents are used to show the parametric dependence.

The perfectly plastic solution approach from Section 2.3 combined with Eq. (18) can be used to approximate the behavior of the stress field as a function of r/a. The result is shown in Fig. 9. The solutions of normalized nominal stress are shown for σ_{nom}/σ_y

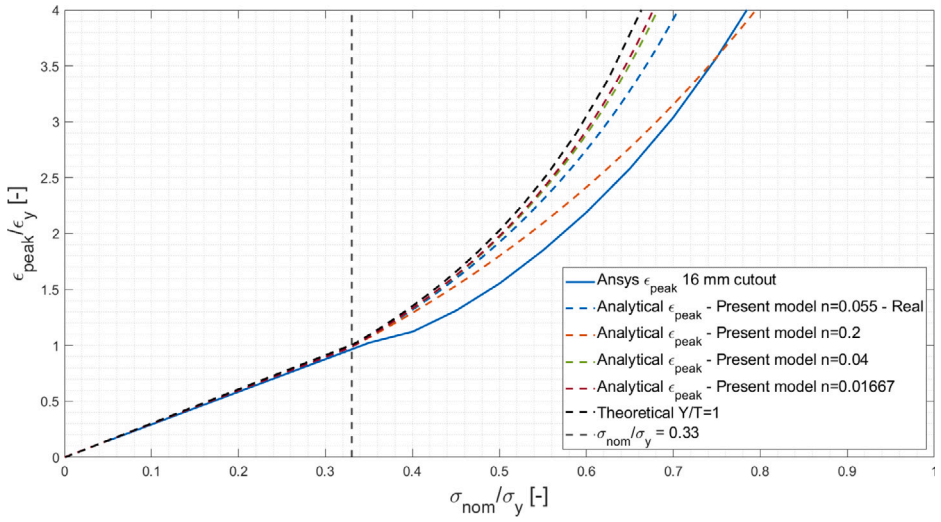

Fig. 8. Normalized local strain as function of normalized nominal stress — analytical versus numerical.

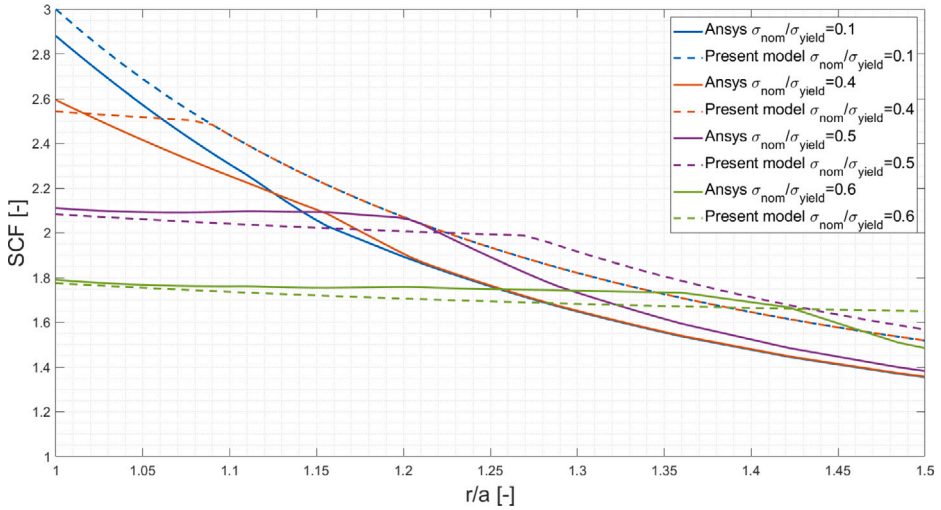

Fig. 9. Numerical and analytical solution elasto-plastic transition over width of the S960 specimen.

values equal to 0.1, 0.4, 0.5, and 0.6. Since the theoretical elastic stress concentration factor for a circular cutout is equal to 3, this is also shown in the figure. The numerical elastic solution when $r/a = 1$ is equal to 2.9 due to the finite width, which is located at $r/a = 30$ in the FEA model. Higher normalized nominal stresses tend to give better agreement between analytical and numerical solutions. As shown in the figure, the shift in the extent of the plastic zone is taken into account.

4. Results

Eq. (9) and (15) were used to convert chosen Y/T ratios and yield strengths into combinations for K and n and vice versa. These K and n values were then converted into stress–strain curves for use in Ansys. To assess the influence of the Y/T ratio, the numerical model is used to examine Y/T ratios equal to 0.6, 0.86, 0.91, and 0.96, which include a value more representative of lower strength steels (0.6, corresponding to a Grade A steel), two that are representative of high-strength steels (0.91 and 0.96, corresponding to a nominal yield strength greater than S690), and one in between.

The yield strength is kept constant at a value of 976.25 MPa. A comparison of the stress fields for different Y/T ratios is shown in Fig. 10. All curves overlap for the $\sigma_{nom}/\sigma_y = 0.11$ condition because each material still behaves elastically at this level of loading, so the Y/T ratio has not yet had an effect. A decrease in the plastic SCF with an increase in the Y/T ratio is shown in this figure for $r/a = 1$ and $\sigma_{nom}/\sigma_y = 0.45$. After the transition to the elastic solution, the global equilibrium causes an opposite trend. A normalized nominal stress of 0.67 shows the same trend. This example with $\sigma_{nom}/\sigma_y = 0.45$ shows that the extent of the plastic zone seems not

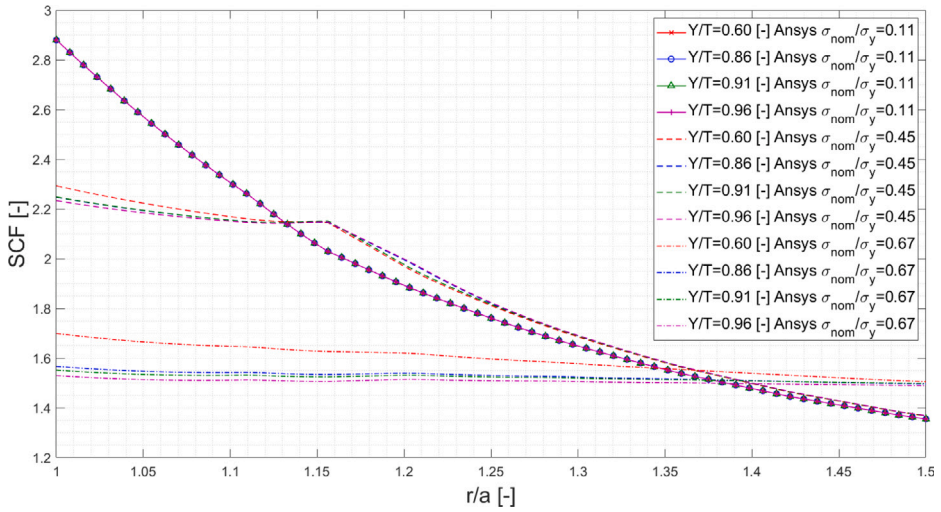

Fig. 10. Numerical solution of elasto-plastic transition over width of specimen with Y/T = [0.6 0.86 0.91 0.96] [–] and σ_y = 976.25 MPa.

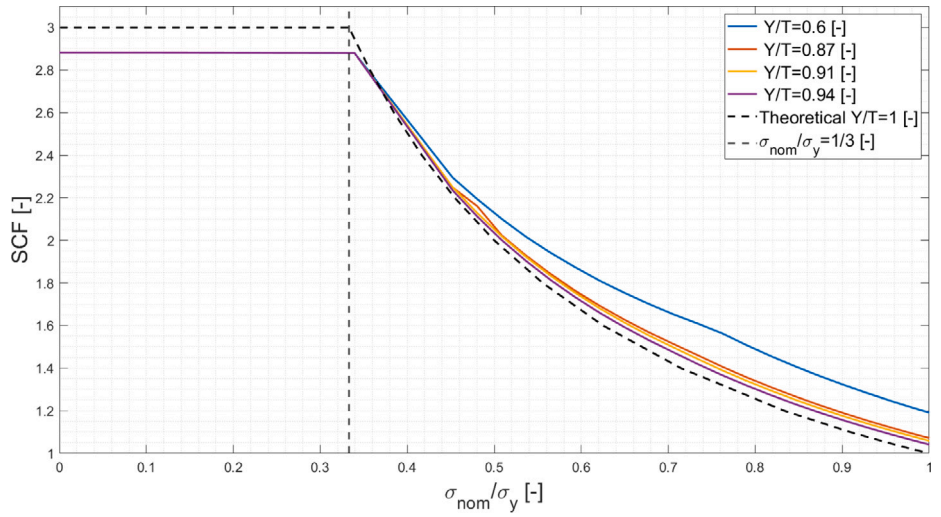

Fig. 11. Numerical solution of SCF as function of normalized nominal stress with varying Y/T.

to be affected by the Y/T ratio. The transition point from plastic into elastic is located at the same value for r/a. This observation, based on numerical results, helps to justify the estimation made in Section 2.3 that a perfectly plastic model can be used. As a result of global equilibrium and plastic redistribution, the SCFs in the plastic zone are higher for a lower Y/T ratio, while the SCFs in the elastic zone are conversely lower for a lower Y/T ratio.

Using the same numerical simulation and plotting SCF as a function of normalized nominal stress at location $r/a = 1$ and $\theta = \pi/2$ results in Fig. 11, which clearly shows that increasing Y/T leads to a decrease in plastic SCF. The perfectly plastic solution for Y/T is also shown to indicate the lower bound.

Extracting the peak strain as the output of the numerical model for a varying Y/T leads to Fig. 12. This figure shows that increasing the Y/T ratio leads to an increase in the normalized peak strain. Quantifying the local strain influenced by the Y/T ratio at $\sigma_{nom}/\sigma_y = 0.67$, the design limit of Bureau Veritas, DNV-GL, and Lloyd's Register [7,8,4], leads to a decrease in plastic SCF equal to 8.5% and a 9.4% increase in local strain, for an increase in Y/T from 0.6 up to 0.87.

At the location $r/a = 1$ and $\theta = \pi/2$, information can be extracted about the influence of the yield strength, as shown in Fig. 13. This figure clearly shows that the yield strength does not have a significant effect on the plastic SCF. Therefore, the effect of the yield strength on the local strain will be insignificant as well.

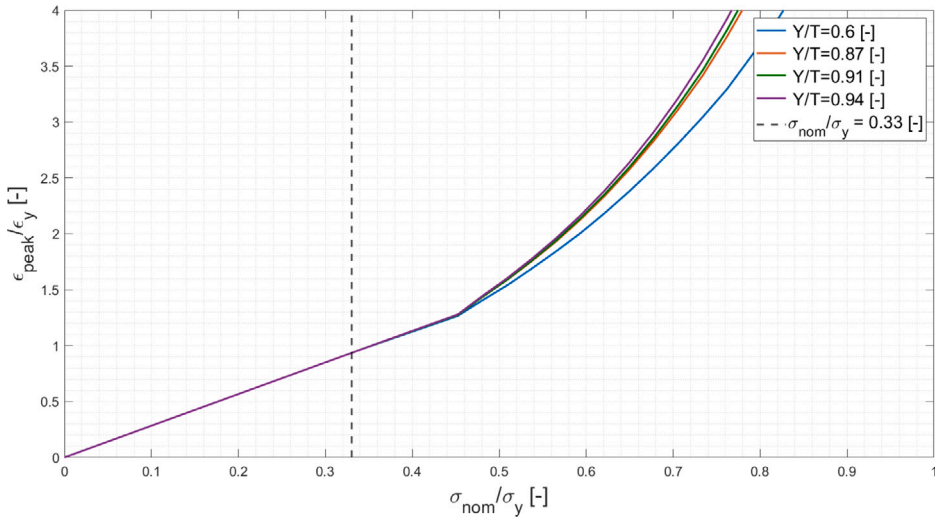

Fig. 12. Numerical solution of normalized local strain as function of normalized nominal stress with varying Y/T ratio.

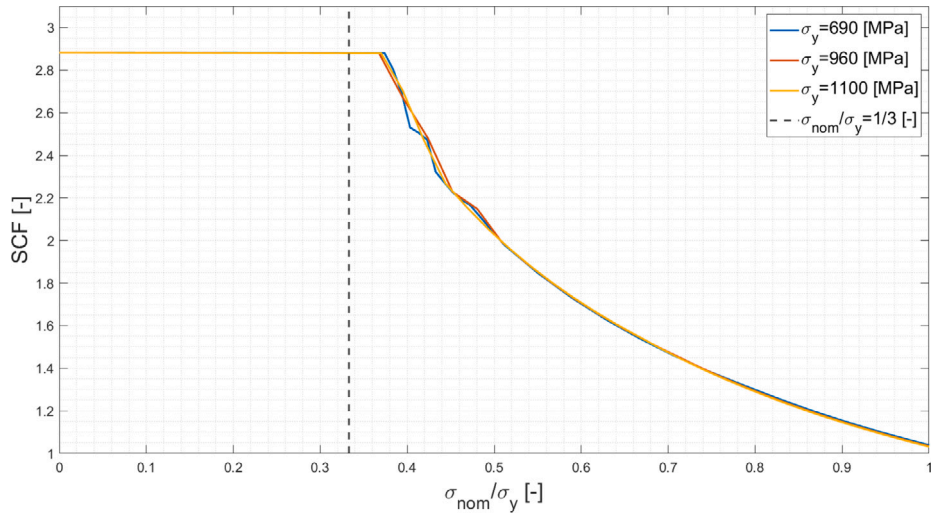

Fig. 13. Numerical solution of SCF as function of normalized nominal stress with varying yield stress.

5. Conclusion

The paper presents a method to analytically approximate the stress/strain field of an infinite plate under tension with a circular hole with a nonlinear plastic material model. A validation study shows that the analytical model approximates the elasto-plastic behavior of high-strength steel with a circular cutout very well. The lower bound of the plastic SCF can be approximated in a theoretical way with the elastic-perfectly plastic solution. The SCF, local strain, and SCF as a function of the specimen's width can be accurately approximated. From the results, it can be concluded that increasing the Y/T ratio leads to a decrease in the plastic SCF for a circular cutout under uniform tension. Moreover, an increase in the Y/T ratio leads to an increase in the local strain and has no effect on the extent of the plastic zone for the materials included in the parametric study. Also, the extent of plastic zone is not affected after increasing the Y/T ratio. An increase in Y/T ratio from 0.87 up to 0.94 leads to a decrease in plastic SCF equal to 2.4% and an increase in local strain equal to 2.8% for a normalized nominal stress equal to $\sigma_{nom}/\sigma_y = 0.67$. An increase in yield strength does not have an effect on the plastic SCF and therefore also does not have an effect on the local strain. Therefore, a Y/T larger than 0.94, which is the limitation according to rules [3–5], results in a marginally increased local strain, which gives a small increase of risk for ductile failure.

Declaration of competing interest

The authors declare that they have no known competing financial interests or personal relationships that could have appeared to influence the work reported in this paper.

Acknowledgments

This research is the result of an M.Sc. thesis project that was undertaken as part of the Joint Industry Research Program known as HYSt: High Y/T Steel. The authors are grateful for the funding provided by the consortium of companies consisting of Bureau Veritas Marine & Offshore SAS, Damen Schelde Naval Shipbuilding BV, Huisman Equipment BV, Lloyd's Register EMEA, POSCO, as well as the Topconsortia voor Kennis en Innovatie (TKI). The authors would like to thank ir. E. Romeijn for providing indispensable knowledge on the application of ultra high-strength steels and guidance throughout the project.

References

[1] Billingham J, Sharp JV, Spurrier J. Research report 105 - Review of the performance of high strength steels used offshore. United Kingdom: HSE Books; 2003.
[2] Billingham J, Healy J, Bolt H. High strength steels - The significance of yield ratio and work-hardening for structural performance. United Kingdom: Energy Institute; 1997.
[3] Lloyd's Register. Rules for the manufacture, testing and certification of materials. London: Lloyd's Register; 2021.
[4] Lloyd's Register. Code for lifting appliances in a marine environment. London: Lloyd's Register; 2021.
[5] DNV-GL. Rules for classification: Ships: Part 2 materials and welding. Oslo: DNV-GL; 2021.
[6] Wong WJ, Walters CL. Failure modes and rules related to the yield-to-tensile strength ratio in steel structures. In: ASME 2021 40th international conference on ocean, offshore and arctic engineering. American Society of Mechanical Engineers; 2021, http://dx.doi.org/10.1115/omae2021-61995.
[7] Bureau Veritas. NR526 rules for the certification of lifting appliances onboard ships and offshore units. Neuilly-sur-Seine: Bureau Veritas; 2021.
[8] DNV-GL. DNVGL-ST-0378 offshore and platform lifting appliances. Edition July 2019. Oslo: DNV-GL; 2020, amended October 2020.
[9] Timoshenko S, Goodier JN. Theory of elasticity. New York: McGraw-Hill Book Company, Inc.; 1951.
[10] Stowell EZ. Technical note 2073: Stress and strain concentration at a a circular hole in an infinite plate. 1950.
[11] Leis BN. Influence of yield-to-tensile strength ratio on failure assessment of corroded pipelines. J Press Vessel Technol 2005;127(November):436–42.
[12] Irwin GR. Plastic zone near a crack and fracture toughness. In: Sagamore research conference proceedings, vol. 4, Syracuse, NY; 1961, p. 63–78.
[13] Hollomon JH. Tensile deformation. Trans Metall Soc AIME 1945;162:268–90.
[14] Kirsch EG. Die Theorie der Elastizität und die Bedürfnisse der Festigkeitslehre. Z Ver Dtsch Ing 1898;42:797–807.
[15] Neuber H. Theory of stress concentration for shear-strained prismatical bodies with arbitrary nonlinear stress-strain law. J Appl Mech 1961;28(4):544–50.
[16] Considère A. Mémoire sur l'emploi du fer et de l'acier. Annales Des Ponts Et Chaussées 1885;9:574–775.
[17] Ansys. Ansys mechanical 2020 R1 (20.1). 2020.
[18] Hradil P, Talja A. Research report VTT-R-04741-16 ductility limits of high strength steels. VTT Technical Research Centre of Finland; 2016.